Structure of C3PO and Mechanism of Human RISC Activation

Xuecheng Ye[1,#], **Nian Huang**[1,#], **Ying Liu**[1], **Zain Paroo**[1], **Carlos Huerta**[1], **Peng Li**[1], **She Chen**[2], **Qinghua Liu**[1,*], and **Hong Zhang**[1,*]

[1] Department of Biochemistry, University of Texas Southwestern Medical Center, Dallas, TX 75390, USA

[2] National Institute of Biological Sciences, No.7 Science Park Road, Zhongguancun Life Science Park, Beijing 102206, China

Abstract

Assembly of the RNA-induced silencing complex (RISC) consists of loading duplex (guide/passenger) siRNA onto and removing the passenger strand from Argonaute (Ago2). Ago2 contributes critically to RISC activation by nicking the passenger strand. Here, we reconstituted duplex siRNA-initiated RISC activity using recombinant human (h)Ago2 and C3PO, indicating a critical role for C3PO in hAgo2-RISC activation. Consistently, genetic depletion of C3PO compromised RNA silencing in mammalian cells. We determined the crystal structure of hC3PO, which reveals an asymmetric octamer barrel consisting of six Translin and two TRAX subunits. This asymmetric assembly is critical for the function of C3PO as a novel endonuclease that cleaves RNA at the interior surface. The current work supports a Dicer-independent mechanism for human RISC activation: 1) Ago2 directly binds duplex siRNA and nicks the passenger strand; 2) C3PO activates RISC by degrading Ago2-nicked passenger strand.

Keywords

RNAi; RISC; Ago2; C3PO; siRNA

INTRODUCTION

RNA interference (RNAi) describes a variety of evolutionarily conserved double-stranded (ds)RNA-initiated gene silencing mechanisms[1–4]. The canonical form of RNAi is initiated

by the ribonuclease (RNase) III Dicer that processes long dsRNA into ~21-nucleotide (nt) small interfering RNA (siRNA). Although nascent siRNA is a duplex, in an active RNA-induced silencing complex (RISC), single-stranded (ss)-siRNA guides the endonuclease Argonaute2 (Ago2) to catalyze sequence-specific cleavage of complementary mRNA[5–7].

Assembly of RISC consists of loading duplex (guide/passenger) siRNA onto Ago2 and dissociation of the passenger strand from Ago2. In *Drosophila melanogaster*, Dicer-2 (Dcr-2) and its dsRNA-binding partner R2D2 coordinately recruit duplex siRNA to dAgo2 to promote RISC assembly[8–13]. The slicer activity of dAgo2 plays a critical role in RISC activation by nicking the passenger strand into 9-nt and 12-nt fragments[14–16]. Chemical modifications that block passenger cleavage also inhibit RISC activation in *Drosophila* embryo and S2 cell extracts[14,16]. In S2 extract lacking dAgo2 activity, RISC assembly, monitored by duplex siRNA unwinding, can only be rescued with wild type, but not catalytic mutant, recombinant dAgo2[17]. In *Neurospora crassa*, the catalytic mutant *qde-2* (homolog of Ago2) strains are defective for duplex siRNA unwinding and RISC activation[18]. These studies establish that Ago2-mediated passenger cleavage is critical for *Drosophila* and *Neurospora* RISC activation.

Recombinant Dcr-2-R2D2 and dAgo2 proteins reconstitute a basal level of dsRNA- and duplex siRNA-initiated RISC activity[17]. This core reconstitution system was used to purify a novel RISC activator from S2 extract named C3PO (component 3 promoter of RISC)[17], which consists of two evolutionarily conserved proteins: Translin/TB-RBP (hereafter Translin for simplicity) and TRAX[19–21]. C3PO is a novel Mg^{2+}-dependent endonuclease that promotes *Drosophila* RISC activation by removing Ago2-nicked passenger strand[17]. In *Neurospora*, a similar function has been proposed for an unrelated exonuclease QIP that degrades QDE-2-nicked duplex siRNA to activate RISC[18].

Among the four mammalian Ago(1–4) proteins, only Ago2 has the slicer activity and is the most critical for siRNA-mediated gene silencing *in vivo*[5,22]. The slicer activity of hAgo2 is required for human RISC activation in crude extract[23]. Chemical modifications impairing passenger cleavage also attenuate duplex siRNA-initiated RISC activity *in vitro* and *in vivo*[24]. These studies suggest that hAgo2-mediated passenger cleavage also plays a critical role in mammalian RISC activation. An alternative "helicase" model for RISC activation is also proposed as several helicases, such as MOV10 and RNA helicase A (RHA), have been genetically implicated in the human RNAi pathway [25–27].

The lack of a robust reconstitution system prevents a clear understanding of the mechanisms of human RISC activation. Neither immunoprecipitated nor recombinant human complex containing Dicer-TRBP (homolog of R2D2) and hAgo2 can catalyze duplex siRNA-initiated RISC activity[28–30]. Although these systems appeared to reconstitute precursor microRNA (pre-miRNA)-initiated RISC activity[28–30], recent studies suggested that this initial observation probably reflected ssRNA-initiated RISC activity as recombinant hAgo2 alone could use intact pre-miRNA as a guide for target mRNA cleavage[23,31]. Here, we have developed a new reconstitution system for duplex siRNA-initiated human RISC activity using Ago2 and C3PO as the core constituents. Moreover, we have solved the X-ray crystal structure of hC3PO, which reveals an asymmetric octamer complex containing six Translin

and two TRAX subunits. The structural and biochemical studies provide important insight into the catalytic mechanism of C3PO and its conserved role in human RISC activation.

RESULTS

Purification of C3PO as a key activator of human RISC

To reconstitute human RISC activity, we generated polyhistidine (His)-tagged Dicer-TRBP and hAgo2 recombinant proteins using an insect cell expression system (Supplementary Fig. 1a). Unlike dAgo2, recombinant hAgo2 displayed potent ss-siRNA-initiated RISC activity (Supplementary Fig. 1b). This distinct feature of hAgo2 presented a problem for the reconstitution study due to background activity resulting from ss-siRNA present in synthetic duplex siRNA (Supplementary Fig. 1c). We could eliminate this background activity by using duplex siRNA prepared with excess (1.5-fold) passenger strand relative to the guide strand (Supplementary Fig. 1c).

Recombinant Dicer-TRBP and hAgo2 could not reconstitute duplex siRNA-initiated RISC activity (Supplementary Fig. 1d), suggesting that other factors are required for human RISC activation. To identify activators of human RISC, we took an unbiased biochemical approach by supplementing recombinant hAgo2 with chromatographic fractions of HeLa extract to reconstitute duplex siRNA-initiated RISC activity. A robust RISC-activating activity was observed in the Q30 fraction (0.3 M salt elution of Q-Sepharose column) of HeLa extract (Supplementary Fig. 1e), which was purified to near homogeneity through a seven-step chromatographic procedure. Two proteins, ~25 kD and ~35 kD, which closely correlated with the RISC-activating activity, were identified as Translin and TRAX by mass spectrometric analysis (Fig. 1a). Since this complex was previously purified from S2 extract as a RISC activator[17], we will refer to human Translin/TRAX complex herein as hC3PO similar to the fly system. The unbiased biochemical purification identified hC3PO as the predominant, if not the only, RISC activator from HeLa extract.

Reconstitution of human RISC activity

Recombinant human Ago2 and C3PO proteins could efficiently reconstitute duplex siRNA-initiated RISC activity in the absence of Dicer-TRBP complex (Fig. 1b and Supplementary Fig. 2a). In this system, the RISC activity was abolished when using a catalytic mutant hAgo2, and C3PO associated with Ago2 in the absence or presence of siRNA (Supplementary Fig. 2b and 2c). Moreover, we compared ds-siRNA- and ss-siRNA-initiated RISC assays by incubating recombinant hAgo2 with or without hC3PO. While hC3PO was necessary for ds-siRNA-initiated RISC activity, it did not enhance ss-siRNA-initiated hAgo2-RISC activity (Fig. 1b). These results suggest that hC3PO functions at the step of RISC assembly rather than the RISC-mediated mRNA cleavage.

In *Drosophila*, Dcr-2-R2D2 complex is absolutely required for recruiting duplex siRNA to dAgo2 for RISC assembly[8]–[12]. However, the role of Dicer-TRBP complex in human RISC activation is controversial. While some studies proposed that Dicer-TRBP promoted human RISC assembly[28]–[30], others suggested that human RISC assembly was uncoupled from dicing and the efficiency of RNAi was not compromised in *dicer* knockout cells[23],[32],[33].

Here, our reconstitution studies indicated that Dicer-TRBP complex was not required for, nor did it enhance the RISC activity of recombinant Ago2 and C3PO (Fig. 1b and 1c). Moreover, recombinant hAgo2, but not dAgo2, could directly bind duplex siRNA independent of the Dicer complex (Fig. 1d). These biochemical studies demonstrate that Dicer-TRBP complex is dispensable for recruiting duplex siRNA to hAgo2 for RISC assembly.

Small hairpin (sh)RNA has been widely used as a potent loss-of-function tool for reverse genetics in mammalian systems[34–36]. Previous reconstitution studies of human RISC commonly used pre-let-7 to initiate RISC assembly[28–30], which carried let-7 miRNA at the 5′ arm of the stem-loop and could function as a guide similar to ss-let-7 to direct hAgo2-mediated mRNA cleavage. To reconstitute shRNA-initiated RISC activity, we designed a modified let-7 shRNA (sh-let-7) by placing let-7 sequence at the 3′ arm of the stem-loop. Since RISC slices its target at the 10-nt position counting from 5′ of guide RNA, unprocessed sh-let-7 could not direct hAgo2 to cleave the same target mRNA for ss-let-7 (Supplementary Fig. 2d). We observed a robust shRNA-initiated RISC activity only when recombinant human Ago2, C3PO, and Dicer-TRBP complex were all present (Fig. 1e). These reconstitution studies suggest that Dicer-TRBP complex is required to process shRNA to duplex siRNA, which is then assembled by Ago2 and C3PO into active RISC.

C3PO is required for efficient RNAi in mammalian cells

We prepared extracts from immortalized wild-type and *translin* (*trsn*)$^{-/-}$ mouse embryonic fibroblasts (MEF) as well as *trsn*$^{-/-}$ MEF expressing a Flag-Translin rescuing transgene. Western blotting showed that Ago2 was equally expressed in different cell lines, whereas the endogenous Translin was missing in *trns*$^{-/-}$ MEF cells (Fig. 2a). TRAX was also presumably missing as previously reported[37]. The lack of C3PO diminished duplex siRNA-initiated RISC activity in *trsn*$^{-/-}$ extract (Fig 2b), which could be rescued by addition of recombinant C3PO or by expression of Flag-Translin in *trns*$^{-/-}$ MEFs (Fig. 2b and 2c). Thus, C3PO is required for efficient duplex siRNA-initiated RISC activity in mammalian extracts.

To determine if C3PO is required for RNAi *in vivo*, we co-transfected wild-type, *trsn*$^{-/-}$, and *trsn*$^{-/-}$ (Flag-Translin) MEFs with a siRNA and a psiCheck2 reporter construct that contained a firefly Luciferase (Fluc) gene as well as a Renilla luciferase (Rluc) gene carrying two perfect target sites in the 3′ untranslated region. Using the ratio of Rluc/Fluc activity to measure the efficiency of RNAi, we observed a four to six-fold derepression of the reporter gene in *trsn*$^{-/-}$ MEFs as compared to wild type MEFs. Moreover, the RNAi defect in *trsn*$^{-/-}$ MEFs could be efficiently rescued by transgenic expression of Flag-Translin (Fig. 2d). Similar to MOV10 or RHA knockdown[26,27], depletion of C3PO resulted in a partial defect of siRNA-mediated gene silencing. Taken together, these studies suggest that the helicase and slicer mechanisms may function redundantly to promote RISC activation in mammalian cells.

Both Translin and TRAX are required for C3PO's nuclease and RISC-activating activities

We compared the binding of recombinant human Translin, TRAX, and C3PO to radiolabeled ssDNA, ss-siRNA, or ds-siRNA by native gel-shift assays (Supplementary Fig. 2a and 3a). Both Translin and hC3PO could efficiently interact with ssDNA and ss-siRNA, but barely with ds-siRNA (Supplementary Fig. 3a). Although TRAX is related to Translin (25% sequence identity and 43% similarity), it exhibited no binding to any substrate (Supplementary Fig. 3a). Like dC3PO[17], hC3PO could efficiently cleave ss-siRNA, but not ds-siRNA (Supplementary Fig. 3b). Additionally, hC3PO exhibited modest nuclease activity toward ssDNA, but not toward 2′-O-methylated oligos (Supplementary Fig. 3b). Moreover, only hC3PO complex, not Translin or TRAX, displayed nuclease activity (Supplementary Fig. 3c). Pre-incubation of Translin and TRAX regenerated ssRNase activity (Supplementary Fig. 3d), suggesting that it was a unique property of C3PO complex, but not of its subunits. Similarly, only C3PO complex, not Translin or TRAX, could function together with hAgo2 to reconstitute duplex siRNA-initiated RISC activity (Supplementary Fig. 3e).

Crystal structure of human C3PO

Since Translin and TRAX are both required for C3PO's activities, it is important to study how these two subunits are assembled in the C3PO complex. Previous X-ray structural studies of human and mouse Translin showed that eight Translin subunits form a football-shaped octameric barrel with a large hollow interior[38],[39]. However, electron microscopic studies suggested a different, open octameric ring structure for Translin[40]. Here we have determined the crystal structure of hC3PO complex at 3.0 A resolution (Table 1), which reveals a hetero-octamer barrel consisting of six Translin and two TRAX subunits with a similar overall architecture as that of Translin homo-octamer (Fig. 3a and 3b)[38],[39]. The two TRAX subunits are located adjacently on one side of the barrel, resulting in an unusual asymmetric structural arrangement (Fig. 3a and 3b).

Both TRAX and Translin subunits are composed of seven α helices, with six of them forming a two-layered right-handed superhelical bundle (Fig. 3c). TRAX also contains several extra loop sequences, of which the N-terminal 30 amino acids and amino acids 157–176 are disordered in the structure. In hC3PO complex, each of the two TRAX subunits forms a heterodimer with a Translin subunit mainly through hydrophobic interactions between the N-terminal α1 helix of TRAX and the α5, α6 helices of Translin, and *vice versa* (Fig. 3d). The conformation of Translin-TRAX heterodimer closely resembles that of Translin-Translin homodimer, with root mean square deviation (RMSD) between superimposed C_α atoms to be ~1.1Å. Nearly all of the interacting residues at the dimer interface are conserved between TRAX and Translin, such as Val35, Phe39, Phe42, and Leu46 of TRAX correspond to Val3, Phe7, Leu10, and Leu14 of Tranlsin (Fig. 3d and Supplementary Fig. 4). The highly conserved and hydrophobic inter-subunit interface strongly suggests that the heterodimer of Translin-TRAX and the homodimer of Translin are the secondary building blocks of C3PO complex.

In hC3PO structure, two Translin-TRAX heterodimers and two Translin-Translin homodimers tetramerize side-by-side to form an asymmetric octameric barrel. The two

TRAX subunits are placed adjacently and interact with each other through their long α1 helices, whereas the α1 helix of Translin always pairs with the α1 helix of Translin (Fig. 3e). Inspection of the TRAX-TRAX interface reveals a network of salt bridges between the two α1 helices, such as Asp51-Arg69′, Glu54-Arg61′ and Lys58-Asp62′ (Fig. 3f). These charged residues are highly conserved in TRAX, but not between TRAX and Translin, which explains why aα1-α1 interface of TRAX-Translin is not favored in hC3PO complex (Supplementary Fig. 4). In contrast, the distances between the charged or polar residues at the three Translin-Translin α1– α1 interfaces are generally too long to allow for the formation of salt bridges or hydrogen bonds (Fig. 3f).

Asymmetric octameric assembly of C3PO

Intriguingly, the stoichiometry of Translin and TRAX is 6:2 in the asymmetric hC3PO complex. At first glance, the hC3PO structure exhibits a four-fold rotational symmetry that relates the top or bottom four subunits, whereas a two-fold symmetry further relates the top and bottom halves of hC3PO. Then, why does TRAX only occupy two out of the eight possible positions of the hetero-octamer? A close inspection of the interactions among the top four subunits (three Translin and one TRAX) reveals a breakdown of the pseudo-four-fold symmetry resulting from a right-handed superhelical shift between adjacent subunits (Fig. 4a). Among the four subunits, TRAX occupies the lowest position (Position 1), and going counterclockwise, the next subunit shifts slightly higher than the last until Translin (Position 4) comes back to encounter TRAX. Consequently, the position of Translin (4) is two helical turns higher relative to that of TRAX, leading to a breakdown of the pseudo-four-fold symmetry (Fig. 4a).

This breakdown of symmetry can be best illustrated by the disruption of the hydrogen bond between Tyr258 of TRAX (corresponding to Tyr210 of Translin) and Asp211 of adjacent Translin subunit. This hydrogen bond is maintained between TRAX and Translin (2), Translins (2) and (3), and Translins (3) and (4), but completely breaks down between Translin (4) and TRAX (Fig. 4a). Instead, it is replaced by new interactions mediated by two highly conserved residues Arg263 and Glu266 of TRAX. Specifically, Arg263 of TRAX forms salt bridges with Asp211′ and Glu207′ of Translin (4), and Glu266 of TRAX interacts with Arg215′ of Translin (3) (Fig. 4a). We also observed a similar spiral arrangement of Translin subunits in the homo-octameric structure of Translin (Supplementary Fig. 5a and 5b), which had not been described in previous reports[38],[39]. Because of this asymmetric spiral arrangement, the position of TRAX subunit is thus unique in the octamer, which may explain why the 6:2 ratio of Translin to TRAX is favored in hC3PO complex.

To determine if this asymmetric assembly is critical for C3PO function, we disrupted the interaction between TRAX and Translin (4) by mutating Arg263 to Asp (R263E) on TRAX, and Asp211 and Glu207 to Ala (D211A, E207A, D211A/E207A) on Translin. Recombinant wild type and mutant hC3PO complexes were produced in *E. coli* by co-expressing His-TRAX and untagged Translin (Supplementary Fig. 5c). Thus, only hC3PO complex could be recovered by nickel purification because Translin was untagged and His-TRAX was insoluble when expressed alone. These mutations significantly affected the oligomeric state of hC3PO, with E207A, R263E, and E207A/D211A mutants showing increasing amount of

large protein aggregates (Fig. 4b). Disruption of the asymmetric octameric assembly severely damaged hC3PO's ssRNA binding and RNase activity (Fig. 4c and 4d). The severity of mutant phenotype was proportional to the percentage of protein aggregates that lacked the RNase activity (Supplementary Fig. 5d).

Catalytic center of C3PO

The RNase activity of hC3PO could be supported by a broad spectrum of divalent ions (e.g. Mg^{2+}, Mn^{2+}), but not by Ca^{2+} or monovalent ions (e.g. Na^+ or K^+) (Supplementary Fig. 6a). Like dC3PO, hC3PO is an endonuclease that could cleave a 21-nt circular ssRNA (Supplementary Fig. 6b). Moreover, the cleavage products migrated slower after phosphatase treatments, suggesting they carried a 5′ phosphate (Supplementary Fig. 6c). Following hC3PO's cleavage of a linear ss-siRNA, the 5′ cleavage products migrated faster by 2-nt after β-elimination treatment, indicative of a 2′, 3-′ hydroxyl terminus (Supplementary Fig. 6c). Therefore, C3PO is an endonuclease that cleaves a phosphodiester bond into a 5′ phosphate and a 3′ hydroxyl terminus.

To further study the catalytic mechanism of hC3PO, we have determined the structure of hC3PO in complex with Mn^{2+}. This new structure is nearly identical to the apo-structure of hC3PO although the two crystals were obtained from different conditions. The anomalous difference electron density map unambiguously reveals the location of a single Mn^{2+} ion (Fig. 5a). Interestingly, there are four extra density peaks in the vicinity of Mn^{2+}, which are likely SO_4^{2-} or PO_4^{3-} ions due to the presence of ammonium sulfate and sodium phosphate in the crystallization condition. Previous bioinformatics studies have predicted three Glu or Asp residues, which are invariant in TRAX but absent in Translin, as the putative catalytic sites of C3PO[17]. Consistently, mutating the corresponding residue E126, E129 or D193 of human TRAX to Ala abolished the RNase activity but did not affect ssRNA binding of hC3PO (Fig. 5b and 5c). These catalytic residues are clustered around the Mn^{2+}, which directly coordinates E129 and E197 of TRAX and one SO_4^{2-}, implicating E197 as the fourth catalytic residue. Indeed, the E197A mutant hC3PO exhibited the same phenotype as the other catalytic mutants. Although the specific roles of E126 and D193 are unclear, one residue could potentially coordinate the metal ion through a water molecule, while the other activates a water molecule to attack the scissile phosphate on ssRNA.

The hC3PO(Mn^{2+}) structure enabled us to model a ssRNA oligo at the catalytic center of hC3PO by superimposing the backbone phosphates onto the positions of the four sulfates/ phosphates (Fig. 5d). In this model, the RNA adopts a standard A-conformation with bases point outward and the phosphate backbone directly contacts several positive charged residues, such as K68, R200 of TRAX and R192 of Translin. Mutating each of these residues to Ala attenuated ssRNA binding and abolished the RNase activity of hC3PO (Fig. 5e and 5f). These mutations did not affect protein folding or complex formation as wild-type and mutant hC3PO exhibited similar profiles on size-exclusion chromatography (Supplementary Fig. 6d). Thus, we conclude that these positively charged residues immediately surrounding the active site are critical for properly positioning ssRNA for catalysis.

C3PO cleaves ssRNA at the interior surface

By size-exclusion chromatography, the estimated size of the endogenous fly or human C3PO was consistent with an octameric complex of six Translin and two TRAX subunits (Supplementary Fig. 7). To determine if C3PO functions as an octamer, we compared the gel-filtration profiles of recombinant hC3PO, ss-siRNA, or a mixture of both in the presence of EDTA (to block catalysis, but not RNA binding) (Fig. 6a). On a carefully calibrated Superdex 200 column, the peak of hC3PO corresponded to ~210 kDa, consistent with an octamer (predicted 226 kDa). When analyzing a hC3PO-ss-siRNA mixture, the peak of hC3PO shifted to ~242 kDa and increased in height, indicating the formation of a hC3PO-ssRNA complex. Consistently, the height of free RNA peak was reduced as a significant amount of ss-siRNA now co-migrated with hC3PO (Fig. 6b). Thus, C3PO binds ssRNA as an octamer.

Notably, all of the catalytic residues are located at the concaved surface of TRAX facing the inside of the hC3PO barrel (Fig. 6c and Supplementary Movie 1). Moreover, the electrostatic potential map illustrated many positively charged residues suitable for nucleotide binding at the interior, but not the exterior, surface of hC3PO barrel (Fig. 6d). Specifically, we showed that K68, R200 of TRAX and R192 of Translin are important for ssRNA binding by hC3PO (Fig. 5d-f). These findings collectively suggest that ssRNA binds to the interior surface of hC3PO complex, where catalysis occurs.

C3PO activates human RISC by degrading Ago2-nicked passenger strand

The slicer activity of human Ago2 is required for converting pre-RISC (Ago2/duplex siRNA) to active RISC (Ago2/guide strand) *in vitro*[23], suggesting that hAgo2-mediated passenger strand cleavage plays a critical role in human RISC activation. However, it remains unclear how Ago2-nicked passenger strand is dissociated from the guide strand to activate RISC. In theory, there are at least three possible mechanisms: 1) passenger fragments spontaneously dissociate; 2) they are unwound by an RNA helicase; 3) they are degraded by an RNase, e.g. C3PO. We have previously shown that mutations of the "EED" catalytic motif of TRAX could abolish dC3PO's RNase activity and its RISC-enhancing activity[17]. Similar results were obtained with the four catalytic mutants (E126A, E129A, D193A or E197A) of hC3PO in our reconstitution studies (Fig. 7a). Additionally, mutations of K68, R200 (TRAX) or R192 (Translin) of hC3PO, which are critical for binding ssRNA for catalysis, also abolished human RISC-activation (Fig. 7b). Collectively, these studies suggest that the RNase activity of C3PO is required for its ability to activate RISC[17].

Because C3PO cleaves ss-siRNA, but not ds-siRNA (Fig. 3b), we hypothesized that that Ago2-mediated passenger cleavage could stimulate the recruitment or activity of C3PO[17]. Consistent with this idea, hC3PO preferred to bind and degrade a nicked duplex siRNA that paired a guide strand with radiolabelled 9-nt and/or 12-nt passenger fragments (Fig. 7c and Supplementary Fig. 8a). We showed that this was not due to spontaneous unwinding of the nicked duplex siRNA followed by binding and cleavage of ssRNA by hC3PO (Supplementary Fig. 8b). Importantly, hC3PO was also required for nicked duplex siRNA-initiated RISC activity, but could not activate hAgo2-RISC when using a nicked duplex siRNA carrying 2′-O-methylated passenger fragments that are resistant to C3PO cleavage

(Fig. 7d and Supplementary Fig. 3b). Thus, the removal of passenger fragments from Ago2 is not a passive process, but requires active degradation by C3PO. These studies strongly suggest that hC3PO facilitates human RISC activation by specifically degrading the Ago2-nicked passenger strand.

DISCUSSION

In the current study, we have purified C3PO as an activator of hAgo2-RISC activity from HeLa extract by chromatographic fractionation. Although many nucleases exist in the crude extract, only C3PO possesses this robust RISC-activation activity. Thus, the unbiased biochemical purification underscores the specific role of C3PO as a key activator of human RISC. Furthermore, we have reconstituted for the first time duplex siRNA-initiated human RISC activity using recombinant Ago2 and C3PO proteins in the absence of Dicer-TRBP complex. It should be noted that more robust RISC activity was obtained with nickel purified hAgo2 than with highly purified hAgo2 recombinant protein following chromatographic purification. Recent studies have implicated heat shock proteins as the molecular chaperones for Ago folding and siRNA loading[41]–[43]. Thus, the nickel-purified hAgo2 preparation might contain insect cell-derived heat shock proteins that could promote hAgo2-RISC activity, but were removed by chromatography. Nevertheless, our previous and current studies establish that C3PO plays an evolutionarily conserved role in *Drosophila* and human RISC activation[17].

Our studies highlight important differences between the fly and human RISC systems. A notable distinction is that hAgo2, but not dAgo2, can be efficiently programmed by ssRNA, such as 21-nt ss-siRNA or 60-nt pre-miRNA, into active minimal RISC. Moreover, Dcr-2-R2D2 complex is absolutely required for recruiting duplex siRNA to dAgo2 for *Drosophila* RISC assembly[9]–[12]. Recombinant Dcr-2-R2D2 and dAgo2 are sufficient to reconstitute the core RISC activity that is greatly enhanced by dC3PO[17]. However, in the absence of Dicer-TRBP complex, recombinant hAgo2 can directly interact with duplex siRNA and function together with hC3PO to reconstitute human RISC activity in the absence of Dicer-TRBP complex. These key differences can be attributed to the unique characteristic of *Drosophila* Ago2 as all four human Ago proteins are more homologous to fly Ago1 than Ago2[23].

It has been established that Ago2-mediated passenger cleavage plays a critical role in RISC activation in flies, fungi, and humans[14]–[16],[18],[23]. The RISC-enhancing activity of C3PO depends on the slicer activity of dAgo2 when using a duplex siRNA-unwinding assay to monitor *Drosophila* RISC assembly[17]. In both fly and human systems, the intrinsic RNase activity of C3PO is required for its ability to activate RISC[17]. Moreover, we observed inefficient RISC assembly accompanied with increased stabilities of passenger strand fragments in C3PO-deficient fly ovary extract, [17]. Here we showed that human C3PO was required for the nicked duplex siRNA-initiated hAgo2-RISC activity. Thus, the removal of Ago2-nicked passenger strand is not a spontaneous process, but requires active assistance from C3PO. Together, our studies support a Dicer-independent mechanism for human RISC activation: 1) hAgo2 directly binds to duplex siRNA, and nicks the passenger strand; 2) hC3PO activates RISC by degrading hAgo2-nicked passenger strand. This Dicer-

independent mechanism may represent a more general model for RISC activation in diverse eukaryotes.

Our structural based mutagenesis studies of C3PO identify four catalytic residues (E126, E129, D193 and E197 of human TRAX) and several key residues (K68 and R200 of TRAX and R192 of Translin) that are critical for binding ssRNA at the catalytic center. The nucleotide binding groove of hC3PO is located at an interface between TRAX and Translin, with residues from both subunits participate in RNA binding and/or catalysis. This also explains why the asymmetric spatial arrangement of TRAX and Translin subunits is critical for C3PO's function.

Both RNA-binding and catalytic residues of C3PO are located inside the football-shaped barrel, suggesting that C3PO may cleave ssRNA at its hollow interior (maximal height 70 Å and diameter 40 Å). However, it is difficult to envision how C3PO recruits ssRNA to the interior of a largely enclosed barrel. An alternative hypothesis is that active C3PO is a tetramer (3 Translin + 1 TRAX). This possibility is less likely because C3PO exists and binds ssRNA as an octamer. Previous studies have shown that Translin also binds ssDNA as an octamer. Notably, a point mutation of *Drosophila* Translin results in a tetrameric form lacking ssDNA-binding activity[44]. It is possible that the oligomeric state of C3PO is more dynamic in solution than in the crystal. C3PO may transiently adopt a tetrameric conformation to contact ssRNA initially, and the nucleotide binding may stabilize the octamer conformation that is required for RNA cleavage.

Previous studies suggest that the interaction between Ago and RNA is a highly dynamic process associated with large conformational changes in both components[45–48]: 1) duplex siRNA is loaded onto Ago2; 2) Ago2-nicked passenger strand has to be removed to activate RISC; 3) target mRNA then comes in to form a duplex with the guide strand; 4) the sliced mRNA products need to dissociate in order for RISC to cleave another target. Therefore, the nicked duplex siRNA is not all deeply buried within Ago2 at all time, and parts of it are accessible to other regulatory factors. We think it is unlikely that the entire nicked duplex siRNA is transferred from Ago2 to the interior of C3PO, where the passenger fragments are degraded and the guide strand is transported back to Ago2. We prefer a model that the guide strand remains bound to Ago2, while the passenger fragments are transferred to the active site of C3PO to be degraded. It is possible that the dissociation and degradation of passenger fragments are closely coupled and jointly promoted by C3PO and Ago2. It will be exciting and challenging for future studies, including structural determination of C3PO-RNA complexes, to unravel the precise mechanism of this dynamic process.

METHODS

Generation of Recombinant Proteins

Wild type and catalytic mutant His-tagged or His-Flag-tagged hAgo2 were expressed in insect cells using a Baculovirus Expression System (Invitrogen) and purified by Nickel and/or Flag-affinity chromatography. Preparation of recombinant dAgo2, Dcr-2-R2D2, and Dicer-TRBP complexes from insect cells were previously described[17, 49]. All wild type and mutant His-tagged Translin, Thioredoxin (Trx)-His-tagged TRAX, and C3PO (co-

expressing His-tagged TRAX and non-tagged Translin) proteins were expressed in *E. coli* BL21 (DE3) and purified with nickel affinity, ion exchange, and gel filtration chromatography. All mutants were constructed using "QuickChange" (Stratagene).

Crystallization and structure determination

Recombinant C3PO complex was prepared as described above and used for crystallization trials. The optimal condition for C3PO crystallization contains 12% PEG3350 and 75 mM potassium citrate (pH 5.4). Single crystals were flash frozen in a cryo-solution containing the crystallizing solution plus 30% ethylene glycol. Diffraction data were collected in-house on a Rigaku FR-E SuperBright generator equipped with VariMax mirror and R-Axis IV++ image plate detector. Data were processed with HKL2000[50]. Molecular replacement was performed with program Phaser[51] in the CCP4 package[52] using human Translin (pdb code 1J1J)[38] monomer as the starting model. The TRAX subunit was manually built, guided by the clear electron density after the Translin subunits were located. The model building and adjustment was performed using Coot[53]. The initial structure refinement was performed using REFMAC5[54] and the final rounds of refinement were completed using Phenix[55]. The crystal used for soaking Mn^{2+} was grown in solution containing 1.2 M ammonium sulfate, 0.1 M phosphate citrate pH 5.4 and 0.4 M lithium sulfate. Single crystals were chosen and soaked in a cryoprotectant containing 2.3 M lithium sulfate and 50 mM manganese sulfate for 3 min and flash frozen in liquid nitrogen. Anomalous diffraction data were remotely collected on beamline ID-19 at Advanced Photon Source, Argonne National Laboratory, IL. The crystal structure was determined by molecular replacement using apo C3PO as initial model, and the refinements were done using similar procedure as apo C3PO crystal structure. The crystal data and the refinement statistics were listed in Table 1. The structural figures were produced using PYMOL[56] and the electrostatic potentials were calculated using APBS[57].

Purification of the RISC-activation activity

Hela cytoplasmic extract (S100) was prepared as previously described[49]. The S100 was loaded onto a HiTrap Q-Sepharose column, and the RISC-activation activity was collected at a step elution Q30 (300 mM NaCl). Ammonium sulfate was added to Q30 to 30% saturation, and after spinning, the supernatant was loaded onto a Phenyl-Sepharose column followed by an elution with 15~0% saturation of ammonium sulfate. After 60% ammonium sulfate precipitation, the pellet containing peak activity was resuspended and loaded onto a Superose 6 gel filtration column. Further purification was performed by sequentially passing the peak activity through a Mono Q column (150~400 mM NaCl), a Heparin column (150~600 mM NaCl), a Hydroxyapatite column (0~200 mM phosphate), and a Smart Q column (150~400 mM NaCl). All purification steps were conducted at 4°C.

In vitro RISC assays, nuclease assays, and native gel shift assays

In vitro RISC assays were carried out essentially as described[17]. Reactions containing recombinant hAgo2, Hela S100 fractions, or MEF cell extracts were incubated at 37°C for 30 minutes except for the time course experiments. Reactions containing dAgo2 were incubated at 30°C. A G-capped labeled 300 nt mRNA containing a perfect let-7 target site

was used as target mRNA (~5 nM, 4×10^4 cpm). 1.5× duplex let-7 siRNA (25 nM), which was prepared with 1.5-fold of passenger strand relative to the guide strand, was used as trigger in duplex siRNA-initiated RISC assays.

All nuclease assays and native gel shift assays were preformed as previously described[17] except for the temperature is 37°C. In native gel shift assays, 10 mM EDTA (final concentration) was added to block the DNA/RNA cleavage. DNA or RNA oligos were radiolabelled at the 5′ end with [γ-^{32}P] ATP by T4 polynucleotide kinase (NEB), or at the 3′ end with [α-^{32}P] pCp by T4 RNA ligase (NEB). A 21-nt circular ss-siRNA was generated by self-ligation of a 5′ radiolabelled ss-siRNA. Radiolabelled let-7 duplex siRNA was prepared by annealing a 5′ radiolabelled strand and 1.5× of unlabelled complementary strand. To prepare the nicked duplex siRNA, the guide strand was annealed with a 9-nt and a 12-nt passenger strand fragments. In different experiments, either the guide strand, or the 9-nt or 12-nt fragment was radiolabelled before annealing.

In vivo RNAi assay

A psiCheck2 reporter system (Promega) was used for *in vivo* RNAi assay. Two perfect target sites for a siRNA (5′-CGAAGGAAGTATCGAATTTAC-3′) were inserted at the 3′ untranslated region (UTR) of the Renilla luciferase (Rluc) gene, with which we could use this siRNA to specifically knockdown Rluc without affecting the Firefly luciferase (Fluc) expression. Wild type and *trsn*$^{-/-}$ primary MEFs were transformed by infecting retrovirus expressing a Ras and a dominant negative p53[58]. In addition, a 3× Flag-tagged human Translin (Flag-Translin) rescuing transgene was introduced into *trsn*$^{-/-}$ MEFs by retrovirus intergration. For *in vivo* RNAi assay, wild type, *trsn*$^{-/-}$, and *trsn*$^{-/-}$ (Flag-Translin) MEFs were co-transfected with the siRNA and the modified psiCheck2 plasmid. A non-specific siRNA (5′-GGAAAGGGCAGAUUGUGUGGA-3′) was used as control. After 24 hours post-transfection, cells were lysed to conduct dual luciferase assays (Promega). The relative luciferase activities were calculated from the ratio of Rluc/Fluc of the specific siRNA-transfected samples compare to that of the control samples.

Western blotting and immunoprecipitation (IP)

Translin antibody was generated against recombinant Translin. The Ago2 antibody was obtained from Millipore. The Actin antibody and Anti-Flag Agarose resin were purchased from Sigma. Western blot and Flag-IP were performed as previously described[59]. For experiments in Fig. 1d, the RISC reactions were prepared by incubating recombinant His-Flag-tagged hAgo2 or dAgo2 with radiolabelled duplex siRNA in absence or presence of, respectively, Dicer-TRBP or Dcr-2-R2D2 complex. After incubated with anti-Flag agarose for 2 hours at 4°C and washed with buffer A containing 0.5 M NaCl, the associated siRNA were extracted by Trizol (Invitrogen), ethanol precipitated, and resolved on a 16% native polyacrylamide gel.

Supplementary Material

Refer to Web version on PubMed Central for supplementary material.

Acknowledgments

References

1. Siomi H, Siomi MC. On the road to reading the RNA-interference code. Nature. 2009; 457:396– 404. [PubMed: 19158785]

2. Liu Q, Paroo Z. Biochemical principles of small RNA pathways. Annu Rev Biochem. 2010; 79:295–319. [PubMed: 20205586]

3. Carthew RW, Sontheimer EJ. Origins and Mechanisms of miRNAs and siRNAs. Cell. 2009; 136:642–55. [PubMed: 19239886]

4. Kawamata, T.; Tomari, Y. Trends Biochem Sci. Making RISC.

5. Liu J, et al. Argonaute2 is the catalytic engine of mammalian RNAi. Science. 2004; 305:1437–41. [PubMed: 15284456]

6. Song JJ, Smith SK, Hannon GJ, Joshua-Tor L. Crystal structure of Argonaute and its implications for RISC slicer activity. Science. 2004; 305:1434–7. [PubMed: 15284453]

7. Rivas FV, et al. Purified Argonaute2 and an siRNA formrecombinant human RISC. Nat Struct Mol Biol. 2005; 12:340–9. [PubMed: 15800637]

8. Liu X, Jiang F, Kalidas S, Smith D, Liu Q. Dicer-2 and R2D2 coordinately bind siRNA to promote assembly of the siRISC complexes. Rna. 2006; 12:1514–20. [PubMed: 16775303]

9. Pham JW, Pellino JL, Lee YS, Carthew RW, Sontheimer EJ. A Dicer-2-dependent 80s complex cleaves targeted mRNAs during RNAi in Drosophila. Cell. 2004; 117:83–94. [PubMed: 15066284]

10. Tomari Y, et al. RISC assembly defects in the Drosophila RNAi mutant armitage. Cell. 2004; 116:831–41. [PubMed: 15035985]

11. Liu Q, et al. R2D2, a bridge between the initiation and effector steps of the Drosophila RNAi pathway. Science. 2003; 301:1921–5. [PubMed: 14512631]

12. Lee YS, et al. Distinct roles for Drosophila Dicer-1 and Dicer-2 in the siRNA/miRNA silencing pathways. Cell. 2004; 117:69–81. [PubMed: 15066283]

13. Tomari Y, Matranga C, Haley B, Martinez N, Zamore PD. A protein sensor for siRNA asymmetry. Science. 2004; 306:1377–80. [PubMed: 15550672]

14. Matranga C, Tomari Y, Shin C, Bartel DP, Zamore PD. Passenger-strand cleavage facilitates assembly of siRNA into Ago2-containing RNAi enzyme complexes. Cell. 2005; 123:607–20. [PubMed: 16271386]

15. Miyoshi K, Tsukumo H, Nagami T, Siomi H, Siomi MC. Slicer function of Drosophila Argonautes and its involvement in RISC formation. Genes Dev. 2005; 19:2837–48. [PubMed: 16287716]

16. Rand TA, Petersen S, Du F, Wang X. Argonaute2 cleaves the anti-guide strand of siRNA during RISC activation. Cell. 2005; 123:621–9. [PubMed: 16271385]

17. Liu Y, et al. C3PO, an endoribonuclease that promotes RNAi by facilitating RISC activation. Science. 2009; 325:750–3. [PubMed: 19661431]

18. Maiti M, Lee HC, Liu Y. QIP, a putative exonuclease, interacts with the Neurospora Argonaute protein and facilitates conversion of duplex siRNA into single strands. Genes Dev. 2007; 21:590– 600. [PubMed: 17311884]

19. Aoki K, et al. A novel gene, Translin, encodes a recombination hotspot binding protein associated with chromosomal translocations. Nat Genet. 1995; 10:167–74. [PubMed: 7663511]

20. Aoki K, Ishida R, Kasai M. Isolation and characterization of a cDNA encoding a Translin-like protein, TRAX. FEBS Lett. 1997; 401:109–12. [PubMed: 9013868]

21. Han JR, Gu W, Hecht NB. Testis-brain RNA-binding protein, a testicular translational regulatory RNA-binding protein, is present in the brain and binds to the 3′ untranslated regions of transported brain mRNAs. Biol Reprod. 1995; 53:707–17. [PubMed: 7578697]

22. Meister G, et al. Human Argonaute2 mediates RNA cleavage targeted by miRNAs and siRNAs. Mol Cell. 2004; 15:185–97. [PubMed: 15260970]

23. Yoda M, et al. ATP-dependent human RISC assembly pathways. Nat Struct Mol Biol. 17:17–23. [PubMed: 19966796]

24. Leuschner PJ, Ameres SL, Kueng S, Martinez J. Cleavage of the siRNA passenger strand during RISC assembly in human cells. EMBO Rep. 2006; 7:314–20. [PubMed: 16439995]

25. Nykanen A, Haley B, Zamore PD. ATP requirements and small interfering RNA structure in the RNA interference pathway. Cell. 2001; 107:309–21. [PubMed: 11701122]

26. Meister G, et al. Identification of novel argonaute-associated proteins. Curr Biol. 2005; 15:2149–55. [PubMed: 16289642]

27. Robb GB, Rana TM. RNA helicase A interacts with RISC in human cells and functions in RISC loading. Mol Cell. 2007; 26:523–37. [PubMed: 17531811]

28. Gregory RI, Chendrimada TP, Cooch N, Shiekhattar R. Human RISC couples microRNA biogenesis and posttranscriptional gene silencing. Cell. 2005; 123:631–40. [PubMed: 16271387]

29. Maniataki E, Mourelatos Z. A human, ATP-independent, RISC assembly machine fueled by pre-miRNA. Genes Dev. 2005; 19:2979–90. [PubMed: 16357216]

30. MacRae IJ, Ma E, Zhou M, Robinson CV, Doudna JA. In vitro reconstitution of the human RISC-loading complex. Proc Natl Acad Sci U S A. 2008; 105:512–7. [PubMed: 18178619]

31. Tan GS, et al. Expanded RNA-binding activities of mammalian Argonaute 2. Nucleic Acids Res. 2009; 37:7533–45. [PubMed: 19808937]

32. Kanellopoulou C, et al. Dicer-deficient mouse embryonic stem cells are defective in differentiation and centromeric silencing. Genes Dev. 2005; 19:489–501. [PubMed: 15713842]

33. Murchison EP, Partridge JF, Tam OH, Cheloufi S, Hannon GJ. Characterization of Dicer-deficient murine embryonic stem cells. Proc Natl Acad Sci U S A. 2005; 102:12135–40. [PubMed: 16099834]

34. Paddison PJ, Caudy AA, Bernstein E, Hannon GJ, Conklin DS. Short hairpin RNAs (shRNAs) induce sequence-specific silencing in mammalian cells. Genes Dev. 2002; 16:948–58. [PubMed: 11959843]

35. Paddison PJ, et al. A resource for large-scale RNA-interference-based screens in mammals. Nature. 2004; 428:427–31. [PubMed: 15042091]

36. Cleary MA, et al. Production of complex nucleic acid libraries using highly parallel in situ oligonucleotide synthesis. Nat Methods. 2004; 1:241–8. [PubMed: 15782200]

37. Yang S, et al. Translin-associated factor X is post-transcriptionally regulated by its partner protein TB-RBP, and both are essential for normal cell proliferation. J Biol Chem. 2004; 279:12605–14. [PubMed: 14711818]

38. Sugiura I, et al. Structure of human translin at 2.2 A resolution. Acta Crystallogr D Biol Crystallogr. 2004; 60:674–9. [PubMed: 15039555]

39. Pascal JM, Hart PJ, Hecht NB, Robertus JD. Crystal structure of TB-RBP, a novel RNA-binding and regulating protein. J Mol Biol. 2002; 319:1049–57. [PubMed: 12079346]

40. VanLoock MS, Yu X, Kasai M, Egelman EH. Electron microscopic studies of the translin octameric ring. J Struct Biol. 2001; 135:58–66. [PubMed: 11562166]

41. Iki T, et al. In Vitro Assembly of Plant RNA-Induced Silencing Complexes Facilitated by Molecular Chaperone HSP90. Mol Cell. 2010; 39:282–91. [PubMed: 20605502]

42. Iwasaki S, et al. Hsc70/Hsp90 Chaperone Machinery Mediates ATP-Dependent RISC Loading of Small RNA Duplexes. Mol Cell. 2010; 39:292–9. [PubMed: 20605501]

43. Miyoshi T, Takeuchi A, Siomi H, Siomi MC. A direct role for Hsp90 in pre-RISC formation in Drosophila. Nat Struct Mol Biol. 2010; 17:1024–6. [PubMed: 20639883]

44. Gupta GD, Makde RD, Rao BJ, Kumar V. Crystal structures of Drosophila mutant translin and characterization of translin variants reveal the structural plasticity of translin proteins. FEBS J. 2008; 275:4235–49. [PubMed: 18647346]

45. Wang Y, et al. Structure of the guide-strand-containing argonaute silencing complex. Nature. 2008; 456:209–13. [PubMed: 18754009]

46. Wang Y, et al. Structure of an argonaute silencing complex with a seed-containing guide DNA and target RNA duplex. Nature. 2008; 456:921–6. [PubMed: 19092929]

47. Wang Y, et al. Nucleation, propagation and cleavage of target RNAs in Ago silencing complexes. Nature. 2009; 461:754–61. [PubMed: 19812667]

48. Parker JS. How to slice: snapshots of Argonaute in action. Silence. 2010; 1:3. [PubMed: 20226069]

49. Paroo Z, Ye X, Chen S, Liu Q. Phosphorylation of the human microRNA-generating complex mediates MAPK/Erk signaling. Cell. 2009; 139:112–22. [PubMed: 19804757]

50. Otwinowski, Z.; Minor, W.; Carter, Charles W, Jr. Methods in Enzymology. Vol. 276. Academic Press; 1997. Processing of X-ray diffraction data collected in oscillation mode; p. 307-326.

51. McCoy AJ, et al. Phaser crystallographic software. J Appl Crystallogr. 2007; 40:658–674. [PubMed: 19461840]

52. Collaborative Computational Project Number 4. The CCP4 suite: programs for proteincrystallography. Acta Crystallogr D Biol Crystallogr. 1994; 50(Pt 5):760–3. [PubMed: 15299374]

53. Emsley P, Lohkamp B, Scott WG, Cowtan K. Features and development of Coot. Acta Crystallographica Section D. 2010; 66:486–501.

54. Murshudov GN, Vagin AA, Dodson EJ. Refinement of macromolecular structures by the maximum-likelihood method. Acta Crystallogr D Biol Crystallogr. 1997; 53:240–55. [PubMed: 15299926]

55. Adams PD, et al. PHENIX: a comprehensive Python-based system for macromolecular structure solution. Acta Crystallogr D Biol Crystallogr. 2010; 66:213–21. [PubMed: 20124702]

56. DeLano, WL. The PyMOL Molecular Graphics System. DeLano Scientific LLC; Palo Alto, CA: 2008.

57. Baker NA, Sept D, Joseph S, Holst MJ, McCammon JA. Electrostatics of nanosystems: application to microtubules and the ribosome. Proc Natl Acad Sci U S A. 2001; 98:10037–41. [PubMed: 11517324]

58. Zou X, et al. Cdk4 disruption renders primary mouse cells resistant to oncogenic transformation, leading to Arf/p53-independent senescence. Genes Dev. 2002; 16:2923–34. [PubMed: 12435633]

59. Ye X, Paroo Z, Liu Q. Functional anatomy of the Drosophila microRNA-generating enzyme. J Biol Chem. 2007; 282:28373–8. [PubMed: 17666393]
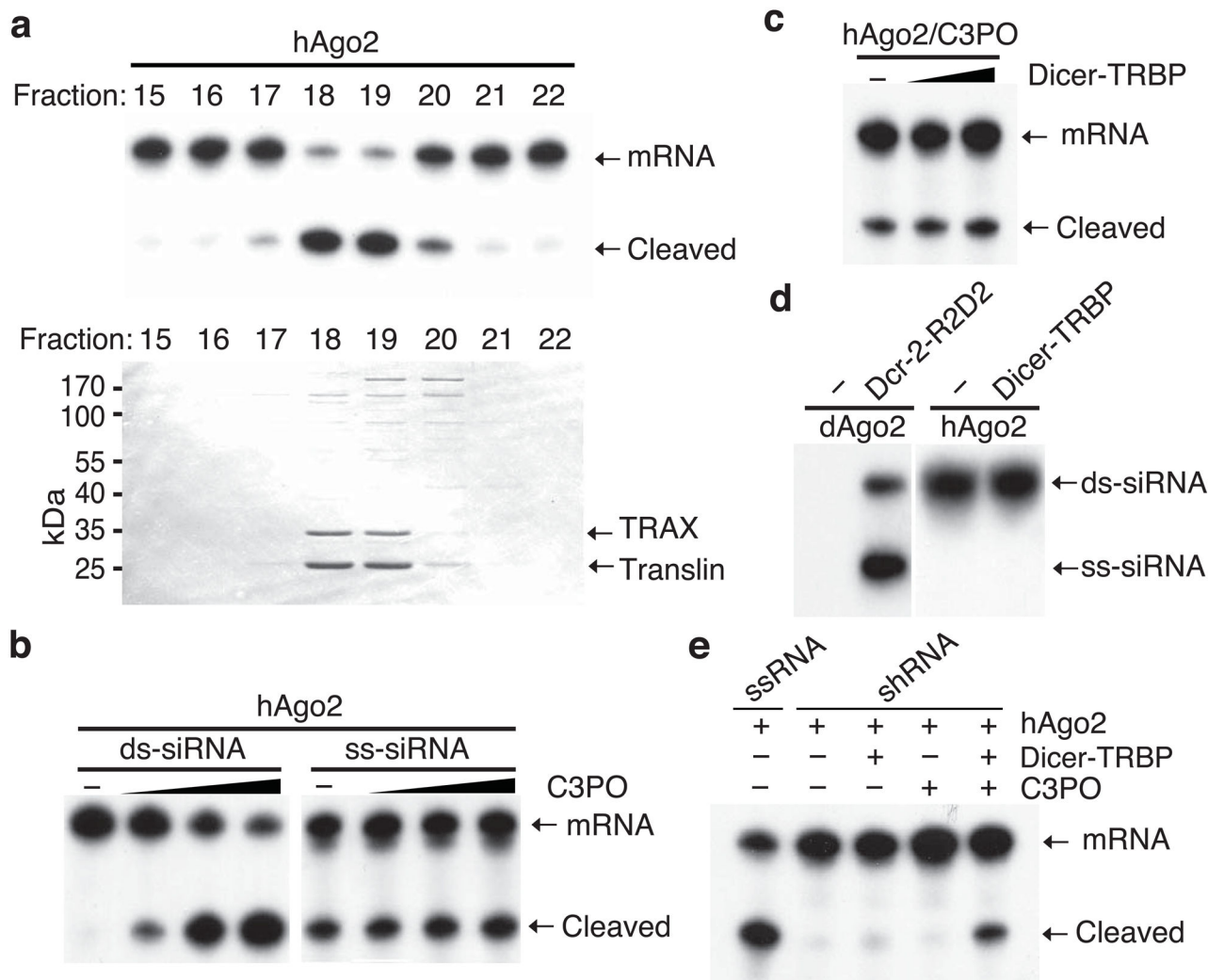
Figure 1. Reconstitution of human RISC activity
(**a**) The duplex siRNA-initiated RISC assays (top) and colloidal stained SDS-PAGE gel (bottom) showing the purified RISC activation activity and correlated proteins.
(**b**) Comparison of C3PO's RISC activation activities using duplex (ds)-siRNA (left 4 lanes) and single-stranded (ss)-siRNA (right 4 lanes) as triggers. While Ago2 concentration was ~0.1 μM, the titration of C3PO was ~0.01, 0.03, and 0.09 μM in this experiment.
(**c**) The duplex siRNA-initiated RISC assays comparing the RISC activities using recombinant hAgo2 and hC3PO in the absence or presence of Dicer-TRBP complex. The relative concentration of Ago2:C3PO:Dicer-TRBP is approximately 1:1:1.
(**d**) Native PAGE gel showing the siRNAs associated with recombinant dAgo2 or hAgo2 in the absence or presence of, respectively, the Dcr-2-R2D2 or Dicer-TRBP complex.
(**e**) Reconstitution of shRNA-initiated RISC activity with various combinations of recombinant Dicer-TRBP complex, hAgo2, and hC3PO.
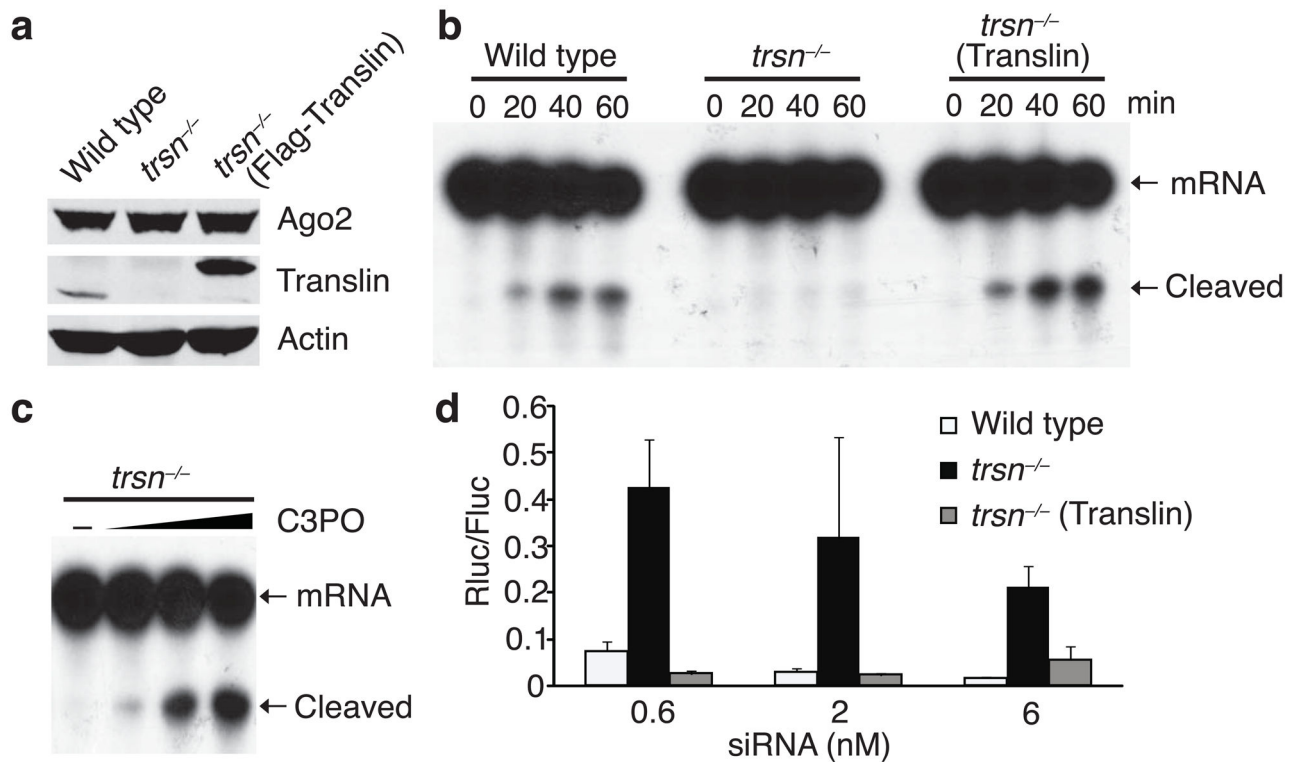
Figure 2. C3PO is required for efficient RNAi in mammalian cells

(**a**) Western blots comparing the levels of endogenous Ago2, Translin, or Actin proteins in wild type, *trsn*^{−/−}, and *trsn*^{−/−} (Flag-Translin) MEF cells.

(**b**) Comparison of the duplex siRNA-initiated RISC activities of the cell lysates prepared from wild-type, *trsn*^{−/−}, and *trsn*^{−/−} (Flag-Translin) MEFs. Protein concentrations were equalized prior to the assays.

(**c**) The deficiency of RISC activity in *trsn*^{−/−} cell extract could be efficiently rescued by addition of recombinant C3PO.

(**d**) A schematic showing the comparison of the *in vivo* siRNA efficiencies between wild-type, *trsn*^{−/−}, and *trsn*^{−/−} (Flag-Translin) MEF cells using different concentration of siRNA. Error bars indicate standard deviations by multiple experiments.
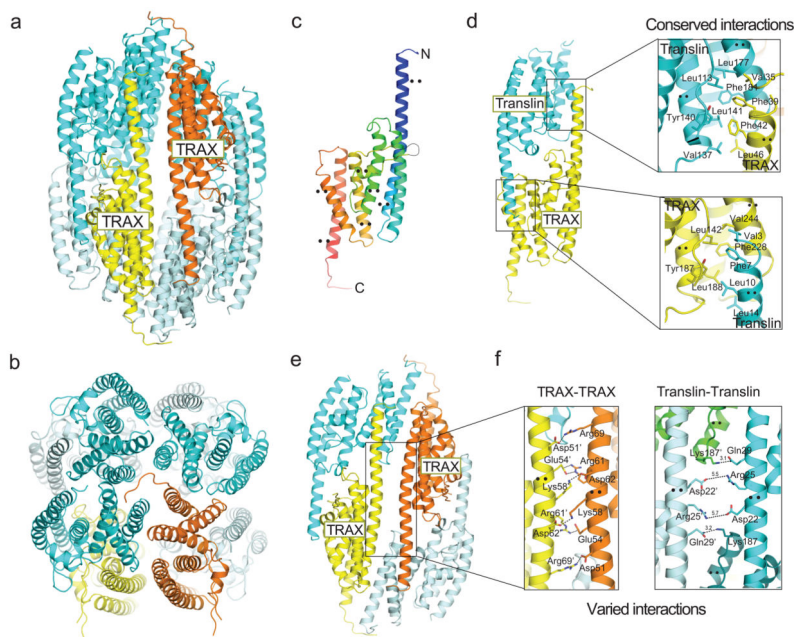
Figure 3. Crystal structure of C3PO

(**a**) Ribbon representation of C3PO complex, in which the two TRAX subunits are colored in yellow and orange, and the six Translin subunits are colored in cyan (top) or light cyan (bottom).

(**b**) An orthogonal view of (a) from the top of C3PO complex.

(**c**) Ribbon representation of human TRAX monomer color ramped from N-terminus (blue) to C-terminus (red). The seven helices in the structure are labeled (α1–α7).

(**d**) Ribbon representation of the TRAX-Translin heterodimer. Two close-up views illustrate in detail the conserved hydrophobic interactions between the α1 helix of TRAX (or Translin) and the α5 and α6 helices of Translin (or TRAX). The bottom close-up view was rotated for 180 degree to compare with the top one.

(**e**) Packing of two TRAX-Translin heterodimer in C3PO complex. The two TRAX subunits contact each other mainly through the α1 helix.

(**f**) A close-up view of the salt bridge network (dotted lines) between the α1 helices of two adjacent TRAX subunits (left). A Translin-Translin interface is shown in comparison (right), illustrating the varied interactions between the two types of interfaces. The distances between selected residues on Translin are also indicated.
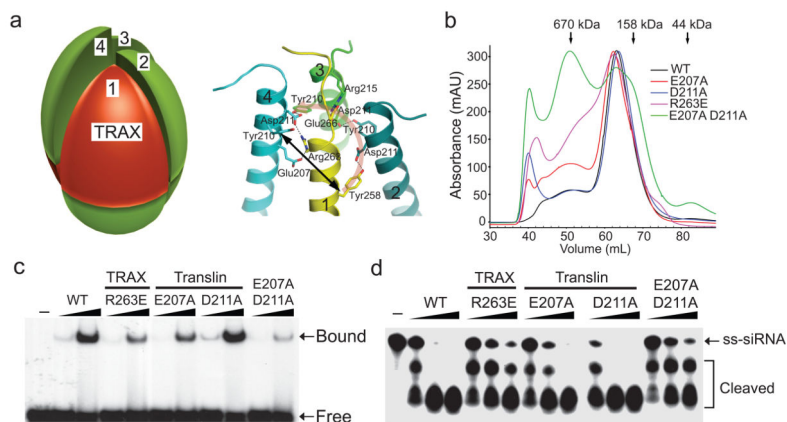
Figure 4. Asymmetric octameric assembly of C3PO

(**a**) (*Left*) A schematic model of C3PO structure illustrating the superhelical shift among the top four (TRAX and three Translin) subunits. (*Right*) A close-up view of specific interactions between TRAX and Translin subunits near the C-terminus. Arg263 of TRAX (1) forms salt bridges throughout with Asp211 and Glu207 of Translin (4), and Glu266 of TRAX (1) interacts with Arg215 of Translin (3). The black arrow indicates the vertical shift between TRAX (1) and Translin (4). The pink arrow indicates the right-handed spiral movement from TRAX (1) to Translin (4).

(**b**) A profiles overlay of Supdex 200 gel filtration chromatography of recombinant wild type (WT), R263E, E207A, D211A, and E207A/D211A mutant C3PO complexes.

(**c**) The native gel shift assays comparing the ability of recombinant wild type and mutant C3PO complexes to bind 5′-radiolabelled ss-siRNA.

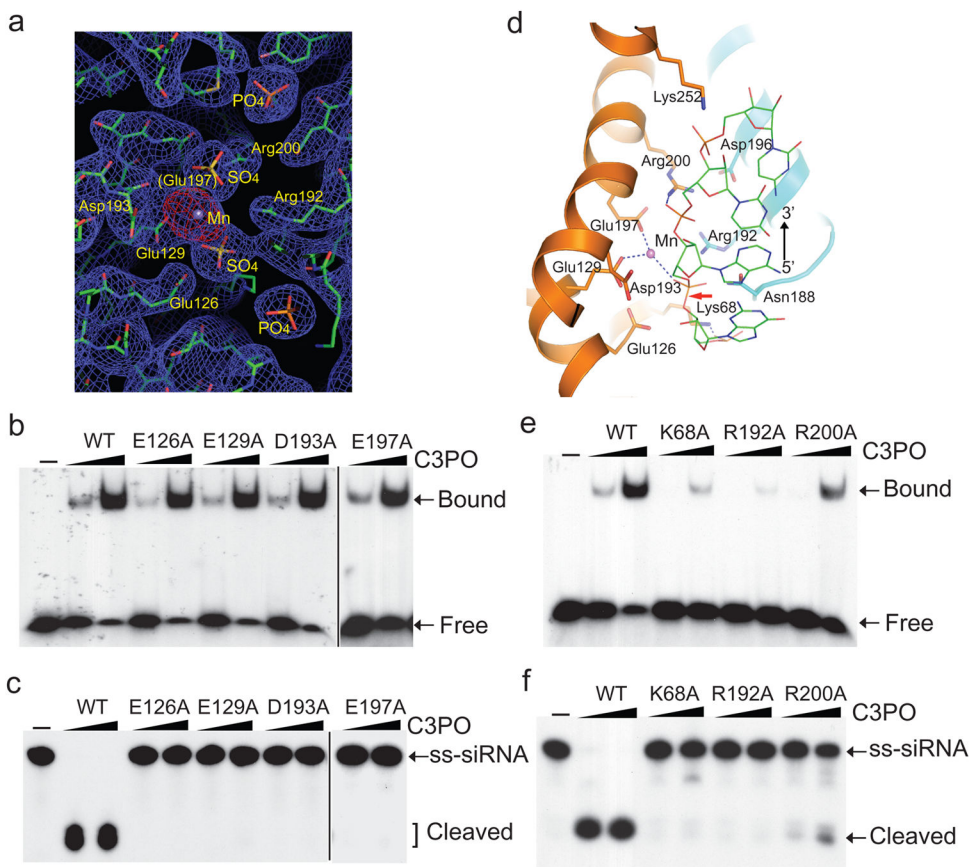(**d**) Comparison of the nuclease activities of recombinant wild type or mutant C3PO complexes.

Figure 5. Catalytic center of C3PO

(**a**) The anomalous difference electron density map unambiguously reveals the locations of a single Mn^{2+} ion as well as two SO_4^{2-} and two PO_4^{3-} ions (distinguished by the presence of small anomalous difference peaks at the sulfur positions). The catalytic residues (E126, E129, D193 and E197 of TRAX) cluster around the Mn^{2+}, which coordinates E129 and E197 of TRAX and one SO_4^{2-} ion.

(**b**) The native gel shift assays comparing the ss-siRNA binding abilities between wild type and four catalytic mutants (E126A, E129A, D193A, E197A) of C3PO.

(**c**) Comparison of the nuclease activities between wild type C3PO and catalytic mutants.

(**d**) A model of ssRNA bound to the active site of C3PO. In this model, the bases of ssRNA point outward, whereas the backbone phosphates directly contact several positive-charged residues, such as R192 of Translin and K68, R200 of TRAX. The red arrow indicates the phosphoester bond that is to be cleaved to generate 5′-phosphate and 3′-hydroxyl products.

(**e**) The native gel shift assays showing the comparison of the ss-siRNA binding abilities between wild type and three mutants (K68A, R192A, R200A) of C3PO.

(**f**) Comparison of the nuclease activities between wild type C3PO and RNA-binding mutants.
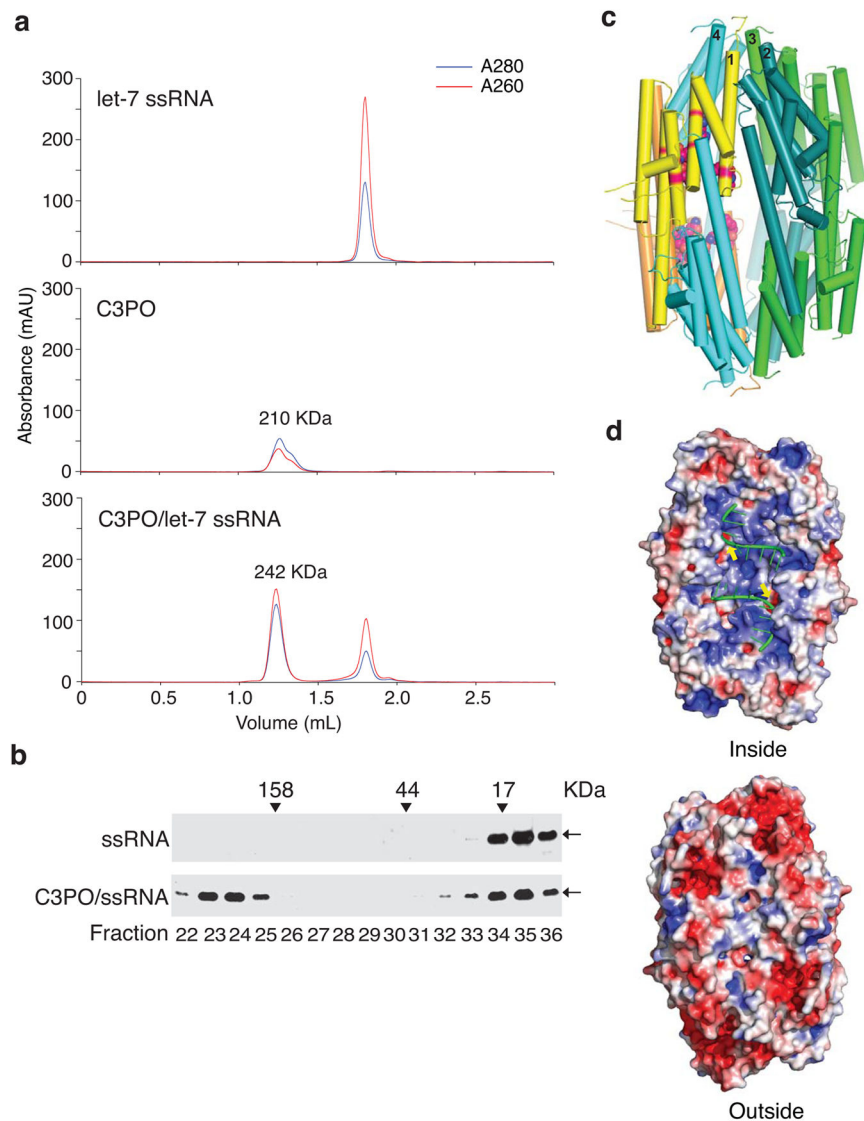
Figure 6. C3PO cleaves ssRNA at the interior surface
(**a**) The Superdex 200 gel filtration profiles of ss-siRNA, recombinant C3PO, a C3PO-ss-siRNA mixture in the presence of 5 mM EDTA (to block catalysis, but not RNA binding).
(**b**) A silver stained Urea-PAGE showing the presence of ss-siRNA in the fractions of Superdex 200 gel filtration chromatography from (a).
(**c**) A cylindrical cartoon representation of human C3PO hetero-octamer. The two TRAX subunits (Position 1) are colored yellow and orange respectively; each Translin subunit is colored differently according to its specific position in the complex. The positions of the four subunits at the top of the barrel are labeled on their C-terminal α7 helices, showing the relative vertical shift between each subunit. The ssRNA binding and catalytic residues of C3PO are located at the inside of the barrel highlighted by magenta.
(**d**) The electrostatic potential mapped on the inside (upper) and outside (lower) molecular surface of C3PO. Negatively potentials are shown in red and positively potentials are in

blue. The modeled ssRNA strands are shown in green cartoons. Arrows indicate the positions of the two catalytic sites.
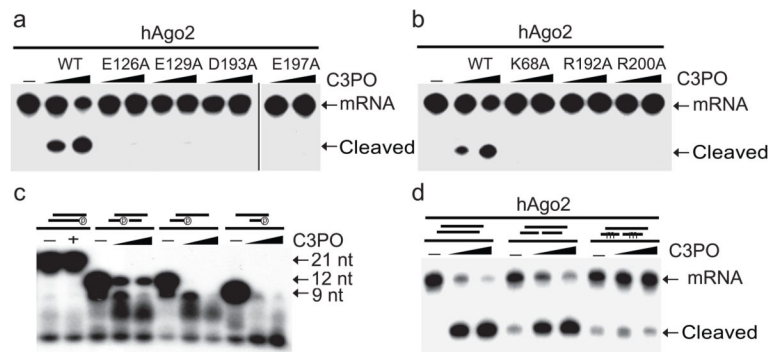
Figure 7. C3PO activates human RISC by degrading Ago2-nicked passenger strand
(**a**) The duplex siRNA-initiated RISC assays comparing the RISC activation activities between recombinant wild type and four catalytic mutants of C3PO.

(**b**) Comparison of the RISC activation activities between recombinant wild type and three RNA-binding mutants of C3PO.

(**c**) The nuclease assays showing the cleavage of duplex siRNA and various nicked duplex siRNAs containing 9-nt and/or 12-nt passenger strand fragments by recombinant C3PO Ⓟ indicates the 5′-radiolabelling.

(**d**) Comparison of the RISC activities of recombinant hAgo2 with or without C3PO using a perfect duplex siRNA, a nicked duplex siRNA, and a nicked duplex siRNA carrying 2′-O-methylated passenger fragments as triggers. indicates 2′-O-methylated RNA.

Table 1

Data collection and refinement statistics

	hC3PO[#]	hC3PO-Mn^{2+}[#]
Data collection		
Space group	C2	P6$_1$22
Cell dimensions		
a, b, c (Å)	171.25, 95.83, 232.89	98.17, 98.17, 98.17
α, β, γ (°)	90.00, 104.58, 90.00	90.00, 90.00, 120.00
Resolution (Å)	30.0-3.00 (3.11-3.00)[*]	50.0-2.94 (3.05-2.94)
R_{sym} or R_{merge}	0.093 (0.683)	0.085 (0.793)
$I/\sigma I$	14.8 (1.90)	51.6 (3.40)
Completeness (%)	99.8 (100.0)	100.0 (100.0)
Redundancy	3.2 (3.1)	20.0 (16.3)
Refinement		
Resolution (Å)	30 – 3.0	50 – 2.94
No. reflections	67135	570754
R_{work}/R_{free}	0.206/0.254	0.219/0.270
No. atoms		
Protein	21056	7019
Ligand/ion	0	23
Water	177	21
B-factors		
Protein	72.83	93.43
Ligand/ion	N/A	98.31
Water	39.88	68.38
R.m.s. deviations		
Bond lengths (Å)	0.012	0.009
Bond angles (°)	0.823	0.616

[#] A single crystal was used for each structure.

[*] Values in parentheses are for highest-resolution shell.